# Hyperbolic metamaterial nanoresonators make poor single-photon sources

Simon Axelrod,[1] Mohsen Kamandar Dezfouli,[1] Herman M. K. Wong,[2] Amr S. Helmy,[2] and Stephen Hughes[1,*]

[1]*Department of Physics, Engineering Physics and Astronomy, Queen's University, Kingston, K7L 3N6 Canada*

[2]*Photonics Group, Edward S. Rogers Sr. Department of Electrical and Computer Engineering, University of Toronto, Toronto, M5S 3H6 Canada*

We study the optical properties of quantum dipole emitters coupled to hyperbolic metamaterial nanoresonators using a semianalytical quasinormal mode approach. We show that coupling to metamaterial nanoresonators can lead to significant Purcell enhancements that are nearly an order of magnitude larger than those of plasmonic resonators with comparable geometry. However, the associated single-photon output $\beta$-factors are extremely low (around 10%), far smaller than those of comparably sized metallic resonators (70%). Using a quasinormal mode expansion of the photon Green function, we describe how the low $\beta$-factors are due to increased Ohmic quenching arising from redshifted resonances, larger quality factors, and stronger confinement of light within the metal. These results explain why hyperbolic metamaterial nanostructures likely make poor choices for single-photon sources.

## I. INTRODUCTION

Engineered cavity structures allow for tight confinement of light and the enhancement of its interaction with matter. In particular, solid-state structures such as photonic crystals [1,2], slow-light waveguides [3], plasmonic nanostructures [4–6], and metamaterial resonators [7,8] allow for the enhancement of the photonic local density of states (LDOS) of embedded quantum emitters, thereby increasing their spontaneous emission rates via the Purcell effect [9]. Such enhancement finds application in areas such as molecule sensing [10], high-resolution imaging [11,12], energy harvesting [13,14], nonlinear optics [15], and single photons [16].

A relatively new class of optical materials known as hyperbolic metamaterials (HMMs) offers the possibility of achieving extreme confinement of light and increased interaction with matter over a broad spectral range [17–19]. Such materials consist of both metal and dielectric parts, and they are typically described as having an anisotropic dielectric tensor within an effective medium description. The dielectric tensor elements $\varepsilon_\parallel$ and $\varepsilon_\perp$ (parallel and perpendicular to the axis of anisotropy, respectively) are of opposite sign, corresponding to metallic or dielectric properties along different axes. For an HMM that is anisotropic along the $z$ axis, for example, the electromagnetic dispersion relation is given by

$$\frac{k_x^2 + k_y^2}{\varepsilon_\parallel} + \frac{k_z^2}{\varepsilon_\perp} = \frac{\omega^2}{c^2}, \tag{1}$$

where $\mathbf{k}$ is the wave vector, $\omega$ is the angular frequency, and $c$ is the speed of light. Since $\varepsilon_\parallel$ and $\varepsilon_\perp$ are of opposite sign, surfaces of constant frequency are hyperbolic, extending to very large values of $k$. The resulting momentum mismatch between HMM and free-space electromagnetic fields results in strong confinement of light around the structure [20]. Moreover, the isofrequency dispersion implies that dipole emitters can couple to a large range of $k$-states at a single frequency, thereby increasing the number of possible decay paths and thus

the spontaneous emission rate [17]. Metamaterial waveguides have also been shown to provide enhanced Purcell factors and Lamb shifts through the associated slow light modes [3].

Many applications in HMM and plasmonic nanophotonics require Purcell enhancements that are radiative in nature [7,8,17,21–24], and it is often of fundamental importance to minimize nonradiative metallic losses. The minimization of such losses is one of the biggest unresolved issues in plasmonics and metamaterial science, limiting nearly every potential application in these fields [25]. While several works have sought to mitigate such losses [25–28], the issue remains an outstanding concern. Despite the importance of analyzing loss in plasmonic and metamaterial resonators, there has been little conclusive analysis of the latter. Several theoretical studies have argued that the Purcell enhancement in simple HMM slabs is radiative in nature [8,17,24], and some experimental work [21] has compared radiative and nonradiative decay in metal and HMM slab structures, but a thorough investigation of quenching in HMMs has not been performed. The role of Ohmic damping has been compared in HMM and metal cavities [29], but energy loss has not. The superior ability of HMMs to engineer radiative decay has also been questioned theoretically [30,31]. An analytical description of radiative and nonradiative decay in HMM and metal resonators is thus of great interest.

In this work, we study metal and HMM nanoresonators for application in single-photon emission, providing a representative analysis of nonradiative loss in such structures. We compare the associated spontaneous emission enhancements and single-photon output $\beta$-factors (the probability of emitting a photon via radiative decay) using a semianalytical Green-function (GF) approach. We first show that the GF of a complex, multilayered HMM resonator can be accurately described in terms of its quasinormal modes (QNMs), the optical modes for an open dissipative cavity structure [32,33]. We report greatly enhanced spontaneous emission rates in HMMs (up to an order of magnitude greater than those of metal resonators with comparable geometry), but surprisingly, significantly lower $\beta$-factors. Using a QNM approach, we show that this increased quenching is due to a combination

*shughes@queensu.ca

of redshifted resonances, larger quality factors, and stronger confinement of light within the metal regions of HMMs. We conclude that HMM resonators are characterized by greatly enhanced Purcell factors that are always accompanied by smaller $\beta$-factors, making them poor choices for single-photon sources and radiative decay engineering.

## II. QUASINORMAL MODE GREEN FUNCTION EXPANSION

The light-matter interactions are rigorously described in terms of the photon GF. For example, the projected LDOS enhancement $\rho(\mathbf{r}_a,\omega)/\rho^h(\mathbf{r}_a,\omega)$ of an $\mathbf{n}_a$-polarized emitter at position $\mathbf{r}_a$ is given by the ratio $\mathrm{Im}\{\mathbf{n}_a \cdot \mathbf{G}(\mathbf{r}_a,\mathbf{r}_a;\omega)\cdot\mathbf{n}_a\}/\mathrm{Im}\{\mathbf{n}_a\cdot\mathbf{G}^h(\mathbf{r}_a,\mathbf{r}_a;\omega)\cdot\mathbf{n}_a)\}$ [34], where $\mathbf{G}$ is the GF and $h$ denotes a homogeneous background medium. Within the weak-coupling regime, the projected LDOS enhancement represents the Purcell factor. Moreover, the GF can be used to quantify the nonradiative decay rate through [5,35]

$$\gamma^{\mathrm{nr}}(\mathbf{r}_a,\omega) = \frac{2}{\hbar\omega\varepsilon_0}\int_V \mathrm{Re}\{\mathbf{j}(\mathbf{r})\cdot\mathbf{G}^*(\mathbf{r},\mathbf{r}_a;\omega)\cdot\mathbf{d}_a\}d\mathbf{r}, \quad (2)$$

where $\mathbf{d}_a = d\mathbf{n}_a$ is the transition dipole of the emitter, and $\mathbf{j}(\mathbf{r}) = \omega\,\mathrm{Im}\{\varepsilon(\mathbf{r},\omega)\}\mathbf{G}(\mathbf{r},\mathbf{r}_a;\omega)\cdot\mathbf{d}_a$ is the induced current density within the scattering geometry.

The GF is known analytically in a few simple cases, but in general it must be obtained numerically. Full numerical solutions of Maxwell's equations can be obtained for a radiating dipole emitter located at position $\mathbf{r}_a$ in a given photonic environment. Using the electric field solution at general positions $\mathbf{r}$, one can obtain the two space-point GF $\mathbf{G}(\mathbf{r},\mathbf{r}_a;\omega)$, [4,36,37], and therefore the LDOS at the dipole location [$\propto \mathrm{Im}\{\mathbf{G}(\mathbf{r}_a,\mathbf{r}_a;\omega)\}$]. Note that one can also obtain the single-photon output $\beta$-factor by calculating the proportion of the total dipole power that is radiated in the far field. However, the dipole approach requires another lengthy simulation to quantify the relevant physics at each new dipole position. Instead, the GF may be expanded in terms of the QNMs of the scattering geometry. The QNMs, $\tilde{\mathbf{f}}_\mu$, are the source-free solution to Maxwell's equations with open boundary conditions [38,39], with a discrete set of complex eigenvalues $\tilde{\omega}_\mu = \omega_\mu - i\gamma_\mu$, and associated quality factors $Q = \omega_\mu/2\gamma_\mu$. Due to the outgoing boundary conditions, QNMs diverge (exponentially) in space [38,40], but their norm is still finite, and can be obtained in a number of complementary ways [41–44].

Within the resonator of interest [38], the transverse part of the GF can be written as an expansion of its QNMs through [39] $\mathbf{G}^{\mathrm{T}}(\mathbf{r},\mathbf{r}';\omega) = \sum_\mu[\omega^2/2\tilde{\omega}_\mu(\tilde{\omega}_\mu - \omega)]\tilde{\mathbf{f}}_\mu(\mathbf{r})\tilde{\mathbf{f}}_\mu(\mathbf{r}')$. For positions near metallic resonators (but outside the regime of quasistatic quenching), the GF can be accurately approximated by the same expansion [45], with the sum greatly reduced to the contribution of one or a few dominant modes near the main cavity resonance [33]. Thus obtaining the dominant QNMs is usually sufficient for obtaining the GF as a function of frequency and position around the resonator. The GF and QNMs can then be used in various quantum optics formalisms [2,35,46], providing the starting point for an analytical and rigorous description of light-matter interactions.
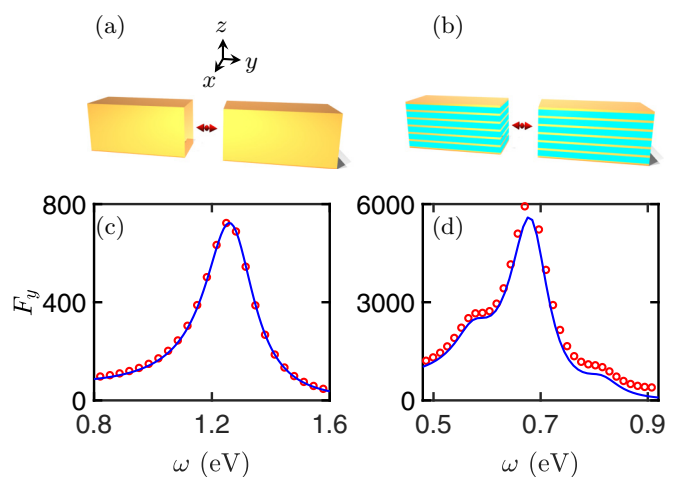


FIG. 1. (a) Schematic of a gold nanodimer resonator. A $y$-polarized quantum dipole is shown in the gap center. (b) Schematic of an HMM dimer with seven layers of gold and six layers of dielectric (blue). (c) Purcell factor for a $y$-polarized dipole in the gap center of a gold nanodimer, obtained with full dipole calculations (red circles) and a QNM expansion (solid blue). (d) Purcell factor as in (c), but for an HMM dimer of metal filling fraction $f_m = 0.2$.

## III. HYPERBOLIC METAMATERIAL NANODIMERS

For practical fabrication purposes we analyze a parallelepiped nanoscale HMM dimer with seven layers of gold and six layers of dielectric, anisotropic along the $z$ axis [Fig. 1(b)], but our general findings below apply to all HMM geometries that we have tried (see below, as well as the Appendix). The dimer configuration enhances Purcell factors in the gap through the bonding effect, and minimizes nonradiative quenching by drawing fields out of the metal [47]. The length of each parallelepiped is 95 nm ($y$ axis), and the width and depth are 35 nm ($x$ and $z$ axes). We fix the gap size at 20 nm in order to maximize the Purcell factor while minimizing nonradiative quenching. We set $\varepsilon = 2.9$ for the dielectric (similar to MgO) and $\varepsilon^h = 2.25$, and we use a Drude model for gold, $\varepsilon(\omega) = 1 - \omega_p^2/[\omega(\omega + i\gamma)]$. We set the plasmon frequency $\omega_p = 1.202 \times 10^{16}$ rad/s and collision rate $\gamma = 1.245 \times 10^{14}$ rad/s, with parameters obtained by fitting experimental data for thin film gold in the frequency regime of interest [48]. The use of a classical permittivity has been shown to be valid for material layers as thin as 1 nm [49–53].

We obtain the QNMs around the resonance of interest for two representative cases: a plasmonic resonator (volume metal filling fraction $f_m = 1.0$) and an HMM resonator with large dielectric character ($f_m = 0.2$). Using COMSOL MULTIPHYSICS [54], we use an iterative frequency-domain pole search with a dipole excitation [55] to obtain the complex eigenfrequencies, and the associated modes are normalized implicitly. We identify a single complex eigenfrequency for the pure gold dimer, $\tilde{\omega}_c/2\pi = 303.29 - i24.18$ THz ($Q = 6.3$). We obtain a maximum Purcell factor of around 720 at the origin (gap center), in excellent agreement with full dipole calculations [Fig. 1(c)]. The HMM dimer response is characterized by three complex eigenfrequencies contributing to the resonance of interest, $\tilde{\omega}_{c_1}/2\pi = 139.215 - i9.847$ THz
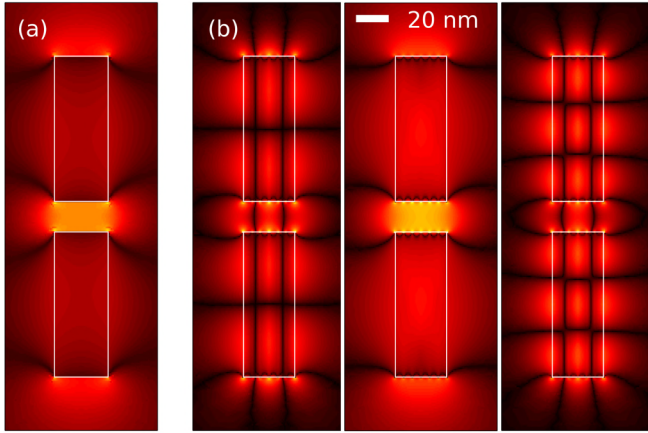
FIG. 2. (a) QNM field profile $|\tilde{\mathbf{f}}_y(0, y, z)|$ for the dominant mode of a plasmonic dimer. The edges of the dimer are shown in white. (b) QNM profile for the three dominant modes of an HMM dimer with filling fraction $f_m = 0.2$, with eigenfrequencies increasing from left to right. Brighter colors indicate stronger fields.

$(Q = 7.1)$, $\tilde{\omega}_{c_2}/2\pi = 165.335 - i\,10.412\,\text{THz}\,(Q = 7.9)$, and $\tilde{\omega}_{c_3}/2\pi = 197.472 - i\,9.860\,\text{THz}\,(Q = 10.0)$. The three-sum QNM maximum Purcell factor at the origin is approximately 5600, which is within 5% of the full dipole result of 5900 [Fig. 1(d); the presence of other nearby modes makes the expansion slightly less accurate than that of the gold dimer—see Appendix A 4]. The HMM and gold QNM profiles are shown in Fig. 2. We remark that the dominant contribution at the origin is from the second QNM, which resembles a localized plasmonic mode; in contrast, modes 1 and 3 resemble Fabry-Pérot resonances, and they contribute strongly at other locations. These results suggest that there is little fundamental difference between plasmonic and HMM modes in nanoresonators, a conclusion that was similarly made for slab structures [30].

Clearly the Purcell factors achievable with the HMM are much higher than those of the pure gold structure (in this case, by an order of magnitude). However, full dipole calculations yield an impressive $\beta$-factor of up to 72% for the metallic resonator, but an extremely poor $\beta$-factor of 12% for the HMM. We have found similarly low $\beta$-factors for different geometries and configurations, including HMM waveguides, and cylindrical nanorods and dimers. We have also found low $\beta$-factors in a spherical HMM cavity, in which Ohmic damping was found to decrease with reduced filling fractions [29], and in an HMM slab structure—see Appendix A 1. To our knowledge, this is the first time that such large losses have been documented in such a wide variety of HMM resonators, and our results stand in contrast to current suggestions in the literature.

## IV. QUASINORMAL MODE DESCRIPTION OF LARGE LOSSES

We argue below that the universally low single-photon $\beta$-factors (quantum efficiencies) associated with HMMs are attributable to three key factors: (a) HMMs confine light to their metal regions more strongly than metallic resonators, (b) HMM modes have higher quality factors than plasmonic
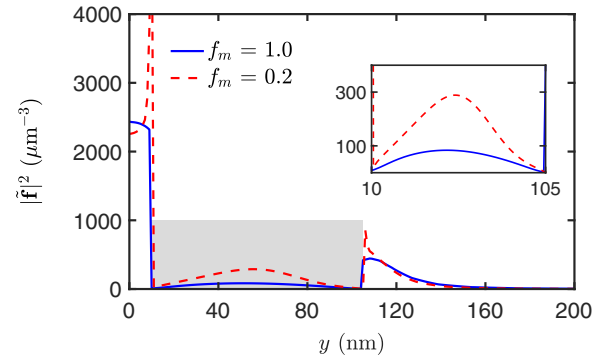


FIG. 3. QNM field strength, $|\tilde{\mathbf{f}}|^2(0, y, 0)$, for the dominant modes of the plasmonic dimer (solid blue) and HMM dimer (dashed red). The shaded region corresponds to positions within each resonator, and specifically to positions within a metal layer of the HMM dimer. Inset: zoom-in of the mode strength for positions inside the resonator.

modes, and (c) HMM resonances are redshifted to regimes of higher metallic loss as the metal filling fraction is reduced. To understand the first two points, we consider Eq. (2) for the case of a $y$-polarized dipole at $\mathbf{r}_a$. Focusing on a single QNM of interest, the total decay rate is proportional to $\text{Im}\{G_{yy}(\mathbf{r}_a, \mathbf{r}_a; \omega)\} = \text{Im}\{A(\omega)\tilde{f}_y^2(\mathbf{r}_a)\}$, where we have defined $A(\omega) = \omega^2/2\tilde{\omega}_c(\tilde{\omega}_c - \omega)$ for the $c$th QNM, and where we have withheld the $c$ dependence of the mode for ease of notation. On the other hand, the nonradiative decay rate given by Eq. (2) scales with $\varepsilon''|A(\omega)|^2|\tilde{f}_y(\mathbf{r}_a)|^2 \int_{\text{metal}} |\tilde{\mathbf{f}}(\mathbf{r})|^2 d\mathbf{r}$, where $\varepsilon'' = \text{Im}\{\varepsilon\}$, and where we have used vertical bars to indicate both an absolute value and the norm of a vector. For $(\text{Im}\{\tilde{f}\}/\text{Re}\{\tilde{f}\})^2 \ll 1$ and $\text{Im}\{\tilde{f}\}/\text{Re}\{\tilde{f}\} \ll Q$, both of which are almost always satisfied in practice, the on-resonance nonradiative coupling $\eta^{\text{nr}} = \gamma^{\text{nr}}/\gamma$ is given by

$$\eta^{\text{nr}} \propto f_m \varepsilon'' Q \langle |\tilde{\mathbf{f}}|^2 \rangle_{\text{metal}}, \qquad (3)$$

where $\langle |\tilde{\mathbf{f}}|^2 \rangle_{\text{metal}} = \int_{V_{\text{metal}}} |\tilde{\mathbf{f}}(\mathbf{r})|^2 d\mathbf{r} / V_{\text{metal}}$ denotes an averaging of the field strength over the metal volume, and we have used $V_{\text{metal}} \propto f_m$ to elucidate the scaling of the nonradiative coupling. Note that the nonradiative decay rate scales with $G^2$, while the total decay rate scales with $G$, so that the nonradiative coupling is increased by an enhancement of $Q|\tilde{\mathbf{f}}|^2$ within the metal, even if the product increases at $\mathbf{r}_a$ as well.

Figure 3 shows the mode strength $|\tilde{\mathbf{f}}(0, y, 0)|^2$ as a function of distance $y$ along the dimer axis, for both $f_m = 1.0$ and 0.2. Outside the dimer, the mode strength is nearly identical for both the metal and the HMM structures, with the only difference occurring a few nm from the metal surface. Within the dimer, however, the mode strength of the HMM is significantly larger than that of the gold resonator. In light of the above discussion, this suggests a much-reduced $\beta$-factor. Evidently, the HMM is not characterized by a stronger modal field at all positions, which would simultaneously increase the Purcell factor while diminishing the $\beta$-factor (see Sec. V). In fact, the enhanced light confinement occurs only within the structure. We can understand this effect as arising from the increased quantity of dielectric within the resonator. Since the dielectric supports the existence of electric fields better than the metal, the field strength within the structure becomes stronger as the metal volume is reduced. The field strength
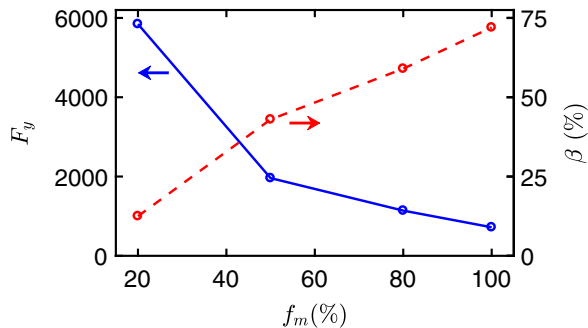
FIG. 4. Midgap on-resonance Purcell factor (solid blue) and output $\beta$-factor (dashed red) for a $y$-polarized dipole at the origin for varying filling fractions. An increase in the Purcell factor is always accompanied by a reduction in the $\beta$-factor.

is enhanced in both dielectric and metal layers, and the latter effect leads to increased loss (see Appendixes A 2 and A 3 for more details). Such an explanation suggests that smaller metal filling fractions are associated with higher loss, which is indeed observed (Fig. 4). We suggest that this effect is characteristic of all resonators consisting of metal and dielectric layers, and it is indeed consistent with all cases we have studied.

The $\beta$-factor is further reduced by an increase in quality factor, $Q^{\mathrm{HMM}}/Q^{\mathrm{metal}} = 1.27$, and from the redshifting of the resonance frequency, since metals with a Drude-like dispersion are characterized by a loss term $\varepsilon'' \propto 1/\omega^3$. Importantly, this latter effect balances the reduction in the metal volume, such that the product $f_m \varepsilon''$ appearing in Eq. (3) is equal to 3.16 for the the HMM dimer, and to 2.59 for the gold dimer (see Appendix A 2). This balancing effect, combined with increased $Q$-factors and enhanced light confinement within the metal, leads to lower $\beta$-factors associated with the HMM dimer.

In light of the above results, we suggest that HMM resonators make poor single-photon sources, for any Purcell factor improvement over metal resonators is accompanied by a reduction in the $\beta$-factor (which renders the photon source increasingly nondeterministic). This somewhat surprising result is expected to be true of all forms of HMM nanoresonators, given the general form of the explanation given above, and we have found it to be true in all of the examples we have studied. Our results also explain why HMM structures can be limited by nonradiative loss in ways that pure metal structures are not.

## V. COMMENTS

As seen in Fig. 3, the QNM strength of the HMM resonator is no larger than that of the metal. The increased $Q$-factor of the HMM yields a small enhancement in the GF, but the effect is rather minor. In fact, the superior HMM Purcell factor is largely due to a decreased resonance frequency. Since the free-space decay rate of a dipole emitter scales with $\omega^3$ [34], the associated spontaneous emission enhancement is larger at lower frequencies. Evidently, HMMs may have difficulty accessing nonperturbative quantum optics effects such as the strong-coupling regime and vacuum Rabi splitting, which rely on an enhanced GF [34], unless they can also be accessed

by metals. Indeed, we have found that vacuum Rabi splitting for a typical quantum dot dipole requires Purcell factors that are orders of magnitude larger than any of the enhancements found here. These results are consistent with those obtained for HMM slab structures [30]. While the strong resonance redshift associated with decreased filling fractions provides an opportunity to finely tune to dipole resonances, such tuning may also be possible by modifying the size of metal resonators [30].

## VI. CONCLUSIONS

We have shown that coupling to HMM nanoresonators can lead to Purcell enhancements that are much larger than those of metals with comparable geometries. Surprisingly, however, we have found that these enhancements are associated with unusually low $\beta$-factors. Using a semianalytical QNM approach, we have shown that these low $\beta$-factors are due to redshifted resonances, increased quality factors, and stronger confinement of light within the metal. We conclude that HMM nanoresonators are likely poor choices for single-photon sources, as well as for many optical applications requiring strong radiative coupling.

## APPENDIX

### 1. Purcell and $\beta$-factors for two different HMM structures

To provide additional generality to the results in the main text, here we present computational results for the Purcell and $\beta$-factors associated with two completely different HMM and metal structures, and we show that they are consistent with those of the nanoresonators studied in the main text. We use a slab structure characterized by a continuum of modes to show that low $\beta$-factors seem to be a general feature of HMM structures, and they are not limited to HMM nanoresonators in particular (though we note that the multimode behavior of slab structures is clearly problematic for single-photon applications). We also examine the spherical HMM resonator studied in Ref. [29] to further support the general argument that HMM nanoresonators make poor single-photon sources.

First we compare a gold slab with an HMM slab of 50% metal filling fraction. The width and length of the slab are one micron ($x$ and $y$ directions), and its height is 150 nm ($z$ direction). The HMM consists of five layers of gold and five layers of dielectric, each with a thickness of 15 nm, and we use the same parameters for the dielectric constants as in the main text. We calculate the $\beta$-factors and Purcell factors as a function of frequency for a $z$-polarized dipole located 10 nm from the surface, through a full dipole calculation using Lumerical finite-difference time-domain (FDTD) simulations [47,56]. Since we scan a large region of frequency space
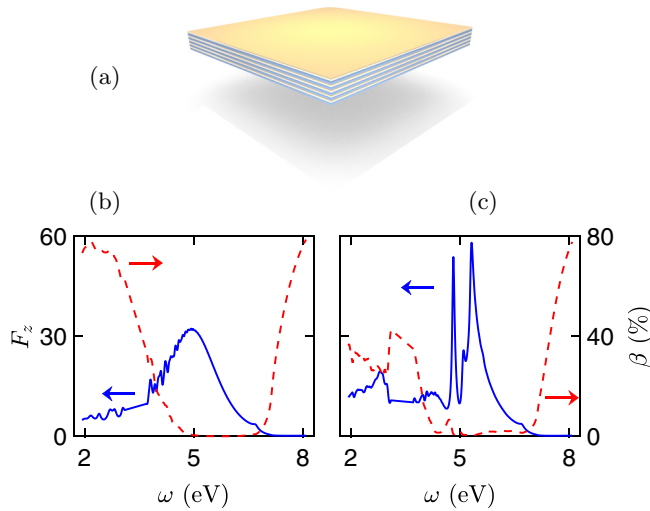
FIG. 5. Comparison of single-photon parameters of a gold slab and an HMM slab of 50% metal filling fraction. (a) Schematic of an HMM slab. (b) Purcell factor and $\beta$-factor for a vertically polarized dipole located 10 nm from the gold slab surface. (c) As in (b), but for an HMM slab of 50% metal filling fraction. For both structures, we see a clear correspondence between Purcell and $\beta$-factors. In particular, the $\beta$-factors are vanishingly small near the main resonances.



FIG. 6. (a) Schematic of an HMM microsphere. (b) Purcell factor (solid blue line) and $\beta$-factor (dashed red line) as a function of metal filling fraction for a $z$-polarized dipole located 10 nm from the outer surface of the sphere. For the larger Purcell factors achievable inside the HMM dielectric regions (not shown), the single photon $\beta$-factors are negligible.

without an obvious modal structure, it is more convenient to use FDTD for these calculations. The FDTD simulations were performed using a 5 nm mesh within a 2 $\mu$m$^3$ computational domain, excluding the 64 perfectly matched layers (PMLs) used to simulate the outgoing boundary condition. The results are shown in Fig. 5. Well below the plasma frequency, the Purcell factor of the HMM is about double that of the gold slab, while the $\beta$-factor of the gold slab is much higher than that of the HMM (around 80% versus 40%). There are higher frequencies for which the HMM Purcell factors are larger, and others for which the gold Purcell factors are larger. However, it is important to note that in these ranges, the $\beta$-factors of each are vanishingly small. In all cases, any enhancement in the Purcell factor is associated with a decrease in the $\beta$-factor, which is in agreement with the conclusion made in the main text.

It is also important to note that the Purcell factors obtained here are orders of magnitude smaller than those of nanoresonator structures. Moreover, it is clear that the Purcell factors represent contributions from a number of resonant modes. A typical requirement for an ideal single-photon source is that dipole emitters couple to a single mode only, with $\beta$- and Purcell factors that are as large as possible. It would thus be preferable, and likely necessary, to use nanoresonators in place of slab structures for such applications. In this context, it is highly desirable to have a modal picture of the underlying physics, in much the same way that one typically analyzes microcavity-enabled cavity-QED effects.

Next we investigate the HMM microsphere studied in Ref. [29], which supports whispering gallery resonances. For this structure, we have used COMSOL MULTIPHYSICS, as in the main text [54]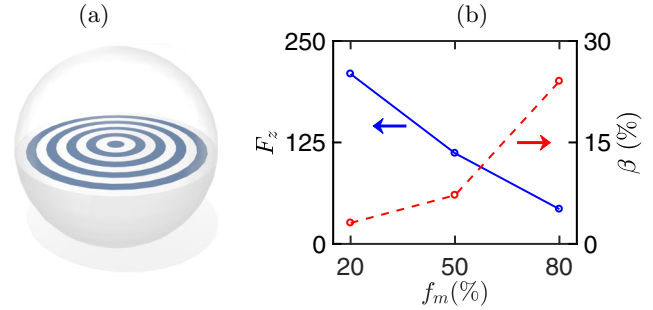. The COMSOL calculations for both the cylindrical resonators (studied in the main text) and spherical geometries (shown here) were performed within a 0.2 $\mu$m$^3$ computational domain for all filling fractions. This domain size included all PML layers. The number of computational elements used for each structure was different in order to meet the different geometrical demands. A minimum of 70 000 elements were used for simulations of pure gold structures, while a maximum of 200 000 elements were used for low filling fraction HMMs. In addition, 10 layers of PML were used in all calculations, which were enough to obtain accurate numerical convergence. The HMM sphere has a radius of 100 nm, and it consists of five layers of silver and five layers of dielectric; further details can be found in Ref. [29]. We obtain $\beta$-factors and Purcell factors for a $z$-polarized dipole located at $z = 10$ nm from the surface of the sphere, coupling to the angular momentum $l = 2$ mode. The results shown in Fig. 6 mirror those of the resonator studied in the main text: the Purcell factor increases and the $\beta$-factor decreases as the filling fraction is reduced. These results are consistent with our general conclusions about nonradiative decay in HMM resonators. In addition, it was concluded in Ref. [29] that Ohmic damping decreases as the filling fraction is reduced, leading to increased quality factors. Evidently this does not lead to less Ohmic loss, for the $\beta$-factor is reduced for smaller filling fractions. This result is consistent with Eq. (3) in the main text, which shows that $\eta^{\mathrm{nr}}$ is actually proportional to $Q$.

### 2. Resonance frequency scaling

In the main text, we argue that the enhanced Purcell factors in HMM nanoresonators are mainly due to a resonance frequency redshift. We note that this redshift leads to a larger loss term through the enhancement of the imaginary part of the dielectric constant. This enhancement is such that that the product $f_m \varepsilon''$ appearing in Eq. (3) of the main text is actually increased. Here we further motivate this result with a simple example.

One can analyze a spherical HMM nanoresonator in the quasistatic approximation, using an effective medium description (see Ref. [29] for the form of the model used). For

a Drude metal and dielectric layers with unit permittivity, the resonance condition is found to be $\omega_0 = \omega_p\sqrt{f_m/3}$. Clearly the resonance frequency is a decreasing function of the metal filling fraction. Moreover, an application of the Drude formula shows that the product $f_m\varepsilon''$ increases as the filling fraction is reduced. This is a direct result of the fact that the imaginary part of $\varepsilon$ scales as $1/\omega^3$, while the real part scales as $1/\omega^2$. This implies that the redshift accompanying the increased Purcell factor yields an increased loss parameter that is large enough to balance the decrease in filling fraction. More generally, one expects that a plasmonic resonance will occur when a denominator of the form $\varepsilon + \alpha\varepsilon^h$ becomes resonant; for some $\alpha$ that depends on the given configuration. For an HMM described as an effective medium, the metal component of the permittivity is given as $\varepsilon = f_m\varepsilon_m + (1 - f_m)\varepsilon_d$ [29]. Satisfying the resonance condition then implies that $\omega_0$ is a decreasing function of $f_m$, and an application of the Drude formula shows that the product $f_m\varepsilon''$ must increase as the filling fraction is reduced.

### 3. Quasistatic picture of diminishing HMM $\beta$-factors

We follow the approach taken in Ref. [57], which makes use of a quasistatic approximation, deemed to be valid for resonators whose dimensions are much smaller than the resonant wavelength. Such an approach becomes increasingly well-justified for HMM nanoresonators, as the size of the resonator remains constant while the resonance frequency is reduced. In the quasistatic limit, the localized modes of a resonator are bound by the following relation:

$$\int_{V_m} -\varepsilon'_m |\tilde{\mathbf{F}}(\mathbf{r})|^2 d\mathbf{r} = \int_{V_d} \varepsilon_d(\mathbf{r}) |\tilde{\mathbf{F}}(\mathbf{r})|^2 d\mathbf{r}. \tag{A1}$$

Here, $\tilde{\mathbf{F}}(\mathbf{r})$ is a "localized field mode," $\varepsilon' = \text{Re}\{\varepsilon\}$, $V_m$ is the metal volume, and $V_d$ is the total dielectric volume (including the volume of the dielectric component of the resonator). The localized mode is defined here as [45]

$$\tilde{\mathbf{F}}(\mathbf{r}) = \int_{V_{\text{dimer}}} \mathbf{G}^h(\mathbf{r},\mathbf{r}';\omega) \cdot \Delta\varepsilon(\mathbf{r}',\omega)\tilde{\mathbf{f}}(\mathbf{r}')d\mathbf{r}' \tag{A2}$$

outside the dimer structure, and

$$\tilde{\mathbf{F}}(\mathbf{r}) = \tilde{\mathbf{f}}(\mathbf{r}) \tag{A3}$$

inside the dimer. Here, $\mathbf{G}^h(\mathbf{r},\mathbf{r}';\omega)$ is the Green function of the homogeneous background medium, $\Delta\varepsilon(\mathbf{r}')$ is the permittivity shift within the dimer, and $\tilde{\mathbf{f}}(\mathbf{r}')$ is the QNM (see the main text). This localized field mode is essentially a regularized QNM, which corresponds to the QNM at positions near the resonator, but it does not diverge in the far field [45].

Invoking the Drude formula for $\omega \ll \omega_p$, and using Eq. (2) of the main text, we obtain the nonradiative decay rate for an $\mathbf{n}_a$-polarized dipole emitter at position $\mathbf{r}_a$:

$$\gamma^{\text{nr}}(\mathbf{r}_a,\omega) = \frac{2d^2\gamma_{\text{col}}|A(\omega)\tilde{F}_a(\mathbf{r}_a)|^2}{\hbar\omega\varepsilon_0} \int_{V_d} \varepsilon_d(\mathbf{r})|\tilde{\mathbf{F}}(\mathbf{r})|^2 d\mathbf{r}, \tag{A4}$$
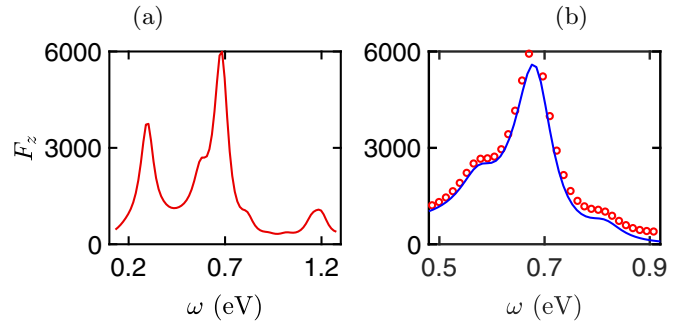


FIG. 7. (a) Extended view of the Purcell factor associated with the HMM nanoresonator studied in the main text, as calculated through full dipole simulations. (b) Purcell factor in the resonant regime of interest, as calculated through full dipole simulations (red circles) and an expansion of three QNMs (solid blue).

where $\gamma_{\text{col}}$ is the collision damping rate in the Drude formula. The on-resonance $\beta$-factor is then

$$\beta = 1 - Q\frac{\gamma_{\text{col}}}{\omega} \int_{V_d} \varepsilon_d(\mathbf{r})|\tilde{\mathbf{F}}(\mathbf{r})|^2 d\mathbf{r}. \tag{A5}$$

We see that the $\beta$-factor decreases as the integrated mode strength over the total *dielectric* volume increases, and as the resonance frequency is reduced. This is precisely what we have observed in HMMs: as the dielectric volume increases, and the resonance frequency drops, the $\beta$-factor decreases. The physical justification for this effect is the same as the one given in the main text. The $\omega^{-1}$ prefactor reflects the fact that lower-frequency regimes are associated with larger loss, while the integral of the field strength over the dielectric regions reflects the fact that stronger fields in the dielectric lead to stronger fields in the metal, and thus to larger losses, as well.

Note that this behavior is different from that of a plasmonic resonator of reduced volume. As the volume is reduced in an ordinary resonator, the resonance frequency becomes blueshifted. However, the smaller volume of the resonator leads to enhanced field strengths both inside and outside the resonator, and thus to larger loss. Both HMM and metal resonators are limited in their increased Purcell enhancement by a reduction in the $\beta$-factor, but the reasons for each are subtly different.

### 4. Multimode behavior of HMM nanoresonators

In the main text, we note that the presence of nearby modes makes the QNM expansion slightly less accurate for the HMM resonator, which may seem surprising given the excellent accuracy of the plasmonic QNM result. For completeness, we have included an extended view of the HMM Purcell factor in Fig. 7, as calculated through full dipole simulations. It is clear that, in addition to the main plasmonic peak near 0.7 eV, as well as the accompanying Fabry-Pérot resonances, there are also interfering modes at higher and lower frequencies. Nevertheless, the three QNM expansion used in the main text is accurate to within 5% in the region of interest near the main peak, as seen in Fig. 7(b).

[1] P. Lodahl, A. F. Van Driel, I. S. Nikolaev, A. Irman, K. Overgaag, D. Vanmaekelbergh, and W. L. Vos, Nature (London) **430**, 654 (2004).

[2] S. Hughes, Opt. Lett. **29**, 2659 (2004).

[3] P. Yao, C. Van Vlack, A. Reza, M. Patterson, M. M. Dignam, and S. Hughes, Phys. Rev. B **80**, 195106 (2009).

[4] P. Yao, V. S. C. Manga Rao, and S. Hughes, Laser Photon. Rev. **4**, 499 (2010).

[5] P. Anger, P. Bharadwaj, and L. Novotny, Phys. Rev. Lett. **96**, 113002 (2006).

[6] M. Frimmer and A. F. Koenderink, Phys. Rev. Lett. **110**, 217405 (2013).

[7] Z. Jacob, J.-Y. Kim, G. V. Naik, A. Boltasseva, E. E. Narimanov, and V. M. Shalaev, Appl. Phys. B **100**, 215 (2010).

[8] M. A. Noginov, H. Li, Y. A. Barnakov, D. Dryden, G. Nataraj, G. Zhu, C. E. Bonner, M. Mayy, Z. Jacob, and E. E. Narimanov, Opt. Lett. **35**, 1863 (2010).

[9] E. M. Purcell, Phys. Rev. **69**, 37 (1946).

[10] J. Homola, S. S. Yee, and G. Gauglitz, Sens. Actuators B **54**, 3 (1999).

[11] K. Kneipp, Y. Wang, H. Kneipp, L. T. Perelman, I. Itzkan, R. R. Dasari, and M. S. Feld, Phys. Rev. Lett. **78**, 1667 (1997).

[12] R. Zhang, Y. Zhang, Z. C. Dong, S. Jiang, C. Zhang, L. G. Chen, L. Zhang, Y. Liao, J. Aizpurua, Y. E. Luo, J. L. Yang, and J. G. Hou, Nature (London) **498**, 82 (2013).

[13] H. A. Atwater and A. Polman, Nat. Mater. **9**, 205 (2010).

[14] Z. Yu, A. Raman, and S. Fan, Proc. Natl. Acad. Sci. (USA) **107**, 17491 (2010).

[15] M. Kauranen and A. V. Zayats, Nat. Photon. **6**, 737 (2012).

[16] D. E. Chang, A. S. Sørensen, E. A. Demler, and M. D. Lukin, Nat. Phys. **3**, 807 (2007).

[17] C. L. Cortes, W. Newman, S. Molesky, and Z. Jacob, J. Opt. **14**, 063001 (2012).

[18] D. R. Smith and D. Schurig, Phys. Rev. Lett. **90**, 077405 (2003).

[19] D. R. Smith, D. Schurig, J. J. Mock, P. Kolinko, and P. Rye, Appl. Phys. Lett. **84**, 2244 (2004).

[20] X. Yang, J. Yao, J. Rho, X. Yin, and X. Zhang, Nat. Photon. **6**, 450 (2012).

[21] J. Kim, V. P. Drachev, Z. Jacob, G. V. Naik, A. Boltasseva, E. E. Narimanov, and V. M. Shalaev, Opt. Express **20**, 8100 (2012).

[22] O. Kidwai, S. V. Zhukovsky, and J. E. Sipe, Opt. Lett. **36**, 2530 (2011).

[23] X. Ni, G. V. Naik, A. V. Kildishev, Y. Barnakov, A. Boltasseva, and V. M. Shalaev, Appl. Phys. B **103**, 553 (2011).

[24] Z. Jacob, I. I. Smolyaninov, and E. E. Narimanov, Appl. Phys. Lett. **100**, 181105 (2012).

[25] J. B. Khurgin, Nat. Nanotech. **10**, 2 (2015).

[26] R. F. Oulton, Nat. Photon. **6**, 219 (2012).

[27] A. Boltasseva and H. A. Atwater, Science **331**, 290 (2011).

[28] L. Rast, T. J. Sullivan, and V. K. Tewary, Phys. Rev. B **87**, 045428 (2013).

[29] C. Wu, A. Salandrino, X. Ni, and X. Zhang, Phys. Rev. X **4**, 021015 (2014).

[30] O. D. Miller, S. G. Johnson, and A. W. Rodriguez, Phys. Rev. Lett. **112**, 157402 (2014).

[31] V. V. Klimov, A. A. Pavlov, D. V. Guzatov, I. V. Zabkov, and V. D. Savinov, Phys. Rev. A **93**, 033831 (2016).

[32] E. S. C. Ching, P. T. Leung, A. M. van den Brink, W. M. Suen, S. S. Tong, and K. Young, Rev. Mod. Phys. **70**, 1545 (1998).

[33] P. T. Kristensen and S. Hughes, ACS Photonics **1**, 2 (2014).

[34] L. Novotny and B. Hecht, *Principles of Nano-Optics* (Cambridge University Press, Cambridge, England, 2006).

[35] R.-C. Ge and S. Hughes, Phys. Rev. B **92**, 205420 (2015).

[36] C. Van Vlack and S. Hughes, Opt. Lett. **37**, 2880 (2012).

[37] V. S. C. Manga Rao and S. Hughes, Phys. Rev. Lett. **99**, 193901 (2007).

[38] P. T. Leung, S. Y. Liu, and K. Young, Phys. Rev. A **49**, 3982 (1994).

[39] K. M. Lee, P. T. Leung, and K. M. Pang, J. Opt. Soc. Am. B **16**, 1409 (1999).

[40] J. U. Nökel and R. K. Chang, in *Cavity-Enhanced Spectroscopies*, edited by R. D. van Zee and J. P. Looney (Academic, San Diego, 2002).

[41] H. M. Lai, P. T. Leung, K. Young, P. W. Barber, and S. C. Hill, Phys. Rev. A **41**, 5187 (1990).

[42] C. Sauvan, J. P. Hugonin, I. S. Maksymov, and P. Lalanne, Phys. Rev. Lett. **110**, 237401 (2013).

[43] P. T. Kristensen, R.-C. Ge, and S. Hughes, Phys. Rev. A **92**, 053810 (2015).

[44] E. A. Muljarov, W. Langbein, and R. Zimmermann, Europhys. Lett. **92**, 50010 (2010).

[45] R.-C. Ge, P. T. Kristensen, J. F. Young, and S. Hughes, New J. Phys. **16**, 113048 (2014).

[46] C. Van Vlack, P. T. Kristensen, and S. Hughes, Phys. Rev. B **85**, 075303 (2012).

[47] R.-C. Ge and S. Hughes, Opt. Lett. **39**, 4235 (2014).

[48] P. B. Johnson and R. W. Christy, Phys. Rev. B **6**, 4370 (1972).

[49] R. Esteban, A. G. Borisov, P. Nordlander, and J. Aizpurua, Nat. Commun. **3**, 825 (2012).

[50] W. Rechberger, A. Hohenau, A. Leitner, J. R. Krenn, B. Lamprecht, and F. R. Aussenegg, Opt. Commun. **220**, 137 (2003).

[51] H. Tamaru, H. Kuwata, H. T. Miyazaki, and K. Miyano, Appl. Phys. Lett. **80**, 1826 (2002).

[52] K. H. Su, Q. H. Wei, X. Zhang, J. J. Mock, D. R. Smith, and S. Schultz, Nano Lett. **3**, 1087 (2003).

[53] J. Zuloaga, E. Prodan, and P. Nordlander, Nano Lett. **9**, 887 (2009).

[54] COMSOL MULTIPHYSICS: www.comsol.com.

[55] Q. Bai, M. Perrin, C. Sauvan, J. P. Hugonin, and P. Lalanne, Opt. Express **21**, 27371 (2013).

[56] Lumerical Solutions: www.lumerical.com.

[57] F. Wang and Y. R. Shen, Phys. Rev. Lett. **97**, 206806 (2006).